Remote estimation of blood pulse pressure via temporal tracking of reflected secondary speckles pattern

Yevgeny Beiderman
Bar-Ilan University
Department of Mathematics
Ramat-Gan 52900, Israel

Israel Horovitz
Natanel Burshtein
Bar Ilan University
School of Engineering
Ramat Gan, 52900, Israel

Mina Teicher
Bar-Ilan University
Department of Mathematics
Ramat-Gan 52900, Israel

Javier Garcia
Vicente Mico
Universitat de València
Departamento de Óptica
c/Dr. Moliner, 50
46100 Burjassot, Spain

Zeev Zalevsky
Bar Ilan University
School of Engineering
Ramat Gan, 52900, Israel

Abstract. We present a novel technique for remote noncontact blood pulse pressure measurement. It is based on tracking both temporal and amplitude changes of reflected secondary speckle produced in human skin when illuminated by a laser beam. The implemented technique extracts the difference between the systolic and the diastolic blood pressure. Experimental results are presented showing good agreement when compared with conventional measurement methods. © *2010 Society of Photo-Optical Instrumentation Engineers*. [DOI: 10.1117/1.3505008]

Keywords: speckle; remote sensing; biomedical optics.

Paper 10043SSRR received Jan. 28, 2010; revised manuscript received Aug. 12, 2010; accepted for publication Aug. 30, 2010; published online Nov. 22, 2010.

1 Introduction

Cardiovascular diseases are considered to be one of the leading cause of death in the modern world and therefore methods for assessing the human cardiovascular condition are of unquestionable interest. Blood pressure is one of four vital signs in health care along with body temperature, heart beat, and respiratory rates. One can divide the techniques of blood pressure measurement into two categories: invasive and noninvasive.[1,2] Invasive methods are expensive, are generally used in hospitals (especially in intensive care units), and require specialists for operation. On the contrary, noninvasive methods reduce medical expenses, are considered to be more friendly to the patient, and are suitable for medical home care. Therefore, noninvasive blood pressure measurement devices have become increasingly common during the last decade as their prices have dropped for end-users.

Optical sensors became popular in biomedical diagnostics. Compared to other types of sensors, numerous advantages of optical sensors have been commonly recognized. One advantage attributed to optical measurement methods is related to their capability of being noninvasive. Another advantage is that these methods are suitable for noncontact applications, making them safer to use since there is no direct electric contact between the sensor and the human body.

Optical sensors are broadly used in heart beats rate and in blood-pressure-related diagnostics. Cardiovascular pulsation causes a change in the amount of blood flux in vessels. Therefore, many optical sensors attempt to measure the variation of the optical power, which is affected by the change in blood flux. The most common method is known as photoplethysmography[3–6] (PPG). PPG is an optical method that monitors the reflected light of an illuminated volume of skin and tissue. Pulsations of the arterial blood cause a variation in the reflected light passing through the tissue. This variation can be monitored at different body locations such as fingertip, earlobe, forehead, etc. As the light passes through the tissue, it becomes slightly modulated by the pulsations of the arterial blood and the amount of light attenuated by the blood varies during heart pumping. When the chambers of the heart contract, blood pressure in the artery increases and diastolic blood pressure changes to systolic blood pressure. The difference between these pressures is called pulse pressure. The PPG technique enables monitoring blood volume pulsation through the skin and, consequently, blood pulse pressure measurement. However, PPG measurements require skin contact and therefore cannot be applied for remote measurements.

Address all correspondance to: Zeev Zalevsky, Bar Ilan University, School of Engineering, Ramat Gan, 52900, Israel. Tel: 972-3-531-7055; Fax: 972-3-910-2625. E-mail: zalevsz@eng.biu.ac.il.

1083-3668/2010/15(6)/061707/7/$25.00 © 2010 SPIE

Another group of techniques includes optical noncontact pulse detection methods, which enable remote measurement. Examples of such methods, are optical interferometry,[7] Doppler-based techniques,[8–10] image processing techniques,[11,12] noncontact PPG,[13] and electronic speckle-pattern interferometry (ESPI) techniques.[14,15] Speckle-based interferometer for biovibration measurement was presented by Tuchin et al.[14] and later applied for cardiovascular pulse detection by Ul'yanov et al.[15]

In general, speckles are self-interference random patterns with a remarkable quality where each individual speckle serves as a reference point from which one can track the changes in the phase of the light that is being scattered from a surface.[16] This is why speckle techniques such as ESPI have been widely used for displacement measurement and vibration analysis (amplitudes, slopes, and modes of vibration) as well as characterization of deformations.[17–23] In the case of object deformation measurement, one can subtract the speckle pattern before the deformation has occurred (due to change in loading, change in temperature, etc.) from the pattern after loading has occurred. This procedure produces correlation fringes that correspond to the object's local surface displacements between the two exposures. From the fringe pattern both the magnitude and the direction of the object's local surface displacement are determined.[18,19]

A special configuration based on usage of a reflected secondary speckle pattern was demonstrated earlier to "hear" remote speech signals and heart beats and to extract vibrations from remote objects.[24,25] The system itself contains a regular camera with its optics as well as a laser source. The laser illuminates the region of interest where the measurement should be performed. Speckles are reflected from the illuminated surface and the speckle pattern is built on the detector of the camera. The optics of the camera is slightly defocused, while this feature is important to convert the tilting movement of the inspected surface into the transversal movement of the speckles[25] (rather the change of this reflected random pattern). This is a remarkable property that causes the speckle pattern to be constant under vibration of the illuminated object and distinguishes it from other speckle-related techniques where the pattern varies in a noncontrollable manner. A shift in the constant speckle pattern, which is caused by vibration of the illuminated object, is tracked by a correlation-based algorithm using MATLAB software.

In previous work, the sound sources or the heart beats were extracted from the spatial movement of the 2-D random speckles pattern.[25] In this paper, we present the way in which this technique can be applied for remote and noninvasive estimation of blood pulse pressure.

To obtain remote estimation of blood pulse pressure we test not only the temporal frequency of the movement but also the amplitude of the movement. The amplitude is important for estimation of the heart beats but also for the blood pressure related parameters. For instance, we studied the shape of the pulse, which can be influenced by many parameters such as tissue and fat layer width as well as the fact that the amount of blood in a specific artery can vary from one person to another.

The shape of the pulse can be easily obtained from the tissue, but it cannot be used to study absolute values for multiple subjects, when the amplitude of the signal is considered. However, as demonstrated in this paper, when the measurement is taken on a certain subject without changing the relative angle between the illuminating laser and subjects' body, a comprehensive study of the amplitude change in the pulse shape can be accomplished. In the experiments performed with a clinical test group, we show that an increased blood pulse pressure results in a larger amplitude measured by the implemented system. Therefore, if a calibration between the measured parameters and the reference of blood pressure is performed at the beginning of each experiment, then a quantitative estimation of pulse pressure can be achieved. This system can perform the measurement at very large distances (even of hundreds of meters), enabling the technology for remote measurement, although in the presented clinical trial, all measurements were performed at a range of about 50 cm.

Section 2 presents the mathematical background. Section 3 describes the experimental setup and test plan. Section 4 presents the obtained results, and Sec. 5 concludes the paper.

2 Mathematical Background

In general, the blood flow can be computed using the following equation:

$$F = \frac{\Delta P\, \pi r^4}{8\nu L}, \tag{1}$$

where ΔP is the pressure difference along a give vessel, L is the length of the vessel, ν is the fluid viscosity, and r is the radius of the vessel tube.

Commonly, two mathematical models are used to model the radial change in a blood vessel. The first is Navier Stokes equations.[26] Generally, it is given by

$$-\frac{\mathrm{d}P}{\mathrm{d}x} = \rho\left(\frac{\mathrm{d}w}{\mathrm{d}t} + u\frac{\mathrm{d}w}{\mathrm{d}r} + w\frac{\mathrm{d}w}{\mathrm{d}r}\right) - \eta\left(\frac{\mathrm{d}^2 w}{\mathrm{d}r} + \frac{1}{r}\frac{\mathrm{d}w}{\mathrm{d}r} + \frac{\mathrm{d}^2 w}{\mathrm{d}x^2}\right), \tag{2}$$

$$-\frac{\mathrm{d}P}{\mathrm{d}r} = \rho\left(\frac{\mathrm{d}u}{\mathrm{d}t} + u\frac{\mathrm{d}u}{\mathrm{d}r} + w\frac{\mathrm{d}u}{\mathrm{d}x}\right) - \eta\left(\frac{\mathrm{d}^2 u}{\mathrm{d}r^2} + \frac{1}{r}\frac{\mathrm{d}u}{\mathrm{d}x^2} + \frac{\mathrm{d}^2 u}{\mathrm{d}x^2} + \frac{u}{r^2}\right), \tag{3}$$

$$\frac{\mathrm{d}u}{\mathrm{d}r} + \frac{u}{r} + \frac{\mathrm{d}w}{\mathrm{d}x} = 0, \tag{4}$$

where P is the pressure in cylinder coordinates along the r (radial) and x (longitudinal) axes, w is the longitudinal velocity of the fluid in the x direction, and u is the radial velocity of the fluid in the r direction. Viscosity is denoted by η and density by ρ. In Eqs. (2) and (3), the terms appearing in the first parentheses represent inertial forces, while the terms in the second pair of parentheses represent viscous forces. Thus, inertial forces minus the viscous losses equals a pressure drop per unit length. Equation (4) presents a continuity equation stating that the net rate of mass influx into any segment of the tube equals the mass storage rate of the segment. No general solution has been presented to Navier-Stokes equations; however, analytic solutions have been calculated for longitudinal flow velocity and longitudinal volume flow in an elastic tube under certain assumptions.[26]

The velocity of the radial expansion of the vessel v, can be derived from the Navier-Stokes equations, as presented by Milnor:[26]

$$v = rC_\alpha \frac{P_d}{\mathrm{d}t}, \tag{5}$$

where v is the radial velocity; r is the radius of the vessel in diastole; P_d is the change in the blood pressure, as of a capillary; and C_α describes the elastic properties of the arterial wall. This can be calculated from Eq. (5), when the blood pressure and the radial velocity of the arterial wall are known.

A relative displacement profile can be calculated by integrating Eq. (5) with respect to time:

$$\mathrm{d}r = rC_\alpha P_d. \tag{6}$$

Therefore, radial displacement dr of the blood vessel linearly depends on the blood pressure difference (systolic minus diastolic).

The second model is presented by Bernoulli's law.[27] For an incompressible flow equation, Bernoulli's law is given in the following form:

$$\tfrac{1}{2}\rho v^2 + \rho g z + P = C, \tag{7}$$

where ρ is a density of the fluid, v is the fluid flow speed at a point on a streamline, g is the acceleration due to gravity, z is the elevation of the point above a reference plan, P is the pressure at the point, and C is an arbitrary constant.

The first term in Eq. (7) represents dynamic pressure, while the second is related to static pressure due to elevation of the fluid. A sum of all pressure terms in Bernoulli's equation remains constant. When considering a pressure drop along the longitudinal x axis, one can assume that the change in z is negligible.

When blood flows in a vessel, pressure losses are generated in the direction of the flow. These pressure losses cause a force F that equals to

$$F = -A\,\mathrm{d}P, \tag{8}$$

where A is the unit area of the arterial vessel, and dP is a change in blood pressure. The direction of F is perpendicular to the cross section of the vessel. The force causes radial extraction of the vessels. Using the second law of Newton mechanics, one can rewrite Eq. (8) in the following way:

$$-A\frac{\mathrm{d}P}{\mathrm{d}x}\,\mathrm{d}x = \frac{\mathrm{d}v}{\mathrm{d}t}\rho A\,\mathrm{d}x, \tag{9}$$

where v is a longitudinal velocity, and ρ is the density of the fluid. One can also rewrite Eq. (9) in the following way:

$$\frac{\mathrm{d}P}{\mathrm{d}x} = \rho\frac{\mathrm{d}v}{\mathrm{d}t}. \tag{10}$$

A possible solution for the extraction of a relative radial displacement was proposed,[27] using same assumptions as were considered in the Navier-Stokes solution by Milnor. Finally, the relative radial displacement (dr) of a vessel is given by

$$\mathrm{d}r \approx \frac{r}{E}\,\mathrm{d}P, \tag{11}$$

where r is the radius of the vessel lumen in diastole, and E is the elastic modulus of the vessel wall. Again, the relative radial displacement is linearly dependant on the pressure difference in a vessel.

In our setup we measured a relative value of displacement of speckle pattern due to change in shape of the vibrating surface. Following the theoretical explanation given by Zalevsky et al. in Ref. 25, a relative displacement is

$$\beta = \frac{4\pi\tan\alpha}{\lambda} \approx \frac{4\pi\alpha}{\lambda}, \tag{12}$$

where β is a relative shift of speckle pattern due to object displacement, α is an angle of tilting of the object, and λ is an optical wavelength. Assuming that the change in the angle is small enough, we obtain a linear proportion between the relative shift and the actual relative radial movement of the blood vessel:

$$\tan\alpha \approx \alpha \approx d, \tag{13}$$

where d is the axial displacement of the vibrating object.

A self-interference pattern was observed by camera (the pattern is constructed on the CCD plane). A temporal change in the pattern is related to a relative spatial shift between two adjacent frames. Using correlation, we extract the relative shift, which is linearly proportional to the tilt of the skin (tangent of the angle between the skin surface and the laser projection).

3 Experimental Setup and Test Planning

The constructed system is presented in Fig. 1, where we see a sketch of the system [Fig. 1(a)], a picture of the camera with its optics and a laser illuminating the hand of the subject [Fig. 1(b)], and a picture captured at a longer exposure to show the illuminating laser beam [Fig. 1(c)]. The setup is very simple and includes only a green laser to illuminate the inspected object (to generate the secondary reflected speckle) and a camera connected to a computer (being slightly defocused) that observes the secondary speckle pattern reflected from the hand of the subject.

The focal length of the optics were 50 mm and the distance from the laser to the subject's hand was about 50 cm. In all of our experiments, the sampling rate of the camera was 300 Hz. We used a green cw laser at a wavelength of 532 nm at an approximate power of 10 mW, and with a stability of $\pm 2\%$. The laser beam incidence angle was chosen to be 90 deg relative to the subject's hand to obtain the smallest possible beam spot size. Therefore, the size of the speckle obtained on the camera was at the largest possible size (at given distance to the camera). Generally, the speckle spot size is linearly proportional to the distance between the object and the imaging device, and inversely proportional to the diameter of that beam spot.

By applying correlation-based tracking, we allocated the position of the 2-D speckles pattern at each instant. We plotted the X and the Y coordinate of the correlation peak shift. Every participant was measured using the implemented system while simultaneously a sleeve-based manual blood measurement device (aneroid sphygmomanometer) was connected to arm to obtain a reliable reference.

Figure 2 presents a temporal signal taken for a short time during clinical tests in which one can see the almost constant peak values that we obtained from the optical measurement. Figures 2(a) and 2(b) are related to two different subjects, while the figures differ in terms of peak polarity (positive or negative). The peak polarity points to the direction of the relative movement of the speckle pattern, where the positive direction refers to a right-hand shift and the negative direction refers to a left-hand shift.

Figures 2(a) and 2(b) are inverted toward each other, but both represent the same pulse shape, where the peak comes before the notch. The dynamic range of the signal (a difference between the peaks, e.g., the highest values, and valleys, e.g., the lowest values) is measured and averaged for this short measurement time, thus providing higher measurement accuracy. The result

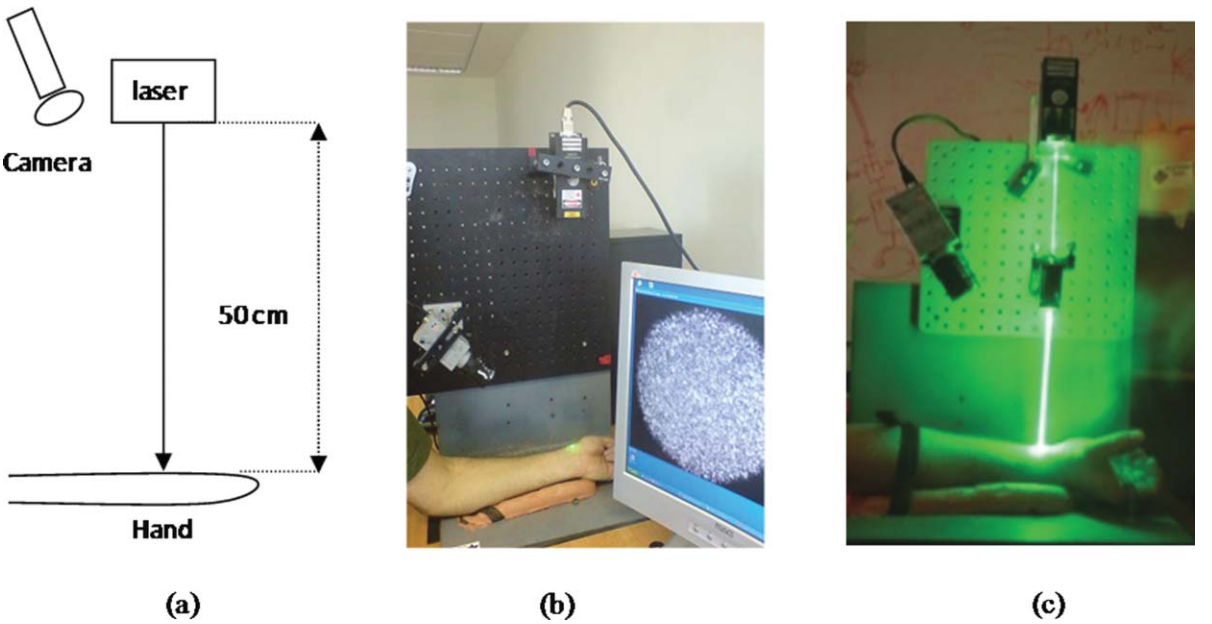

Fig. 1 Implemented optical configuration for remote measurement of blood pressure from a subject's hand: (a) sketch of the optical system, (b) subject's hand under laser illumination as viewed by the camera, and (c) the same as (b) but captured at a longer exposure to show the illuminating laser beam.

is used as an anchor point for correlation measurements and its standard deviation refers to the measurement error. Simultaneously, the actual blood pressure was monitored by taking manual measurements using an air-pressure sleeve device. This procedure was repeated approximately each minute to the end of the individual test.

We had 10 participants in the experiment. Figure 3 shows an example of the measurements obtained from one of those subjects. In the figure, one can see the amplitude of the relative shift of adjacent video frames with speckle pattern (denoted by M) scaled to the values of pressure and the values of manually measured blood pressure (systolic and diastolic). The difference between systolic and diastolic blood pressure is denoted in the figure by Δ, while this parameter is the pulse pressure that we aim to extract using our remote optical monitoring configuration.

A scaling factor was chosen to match two different dimensions estimated by the system and manually measured values, which are in pixel units and pressure (mmHg), respectively. The first values of the measured and the estimated blood pressure were matched.

A correlation coefficient of 0.995 between the estimated and measured values of pulse pressure was achieved using anchor (averaged) points, which are marked by dots on the trend lines. Error bars represent a standard deviation of the anchor points, as calculated from the data shown in Fig. 2.

To obtain a variation of blood pressure in a healthy subject, one was requested to exercise for several minutes. Right after that, the subject was seated in front of the system, while his wrist was illuminated by the laser beam and his arm was connected to the manual blood pressure measurement device. The time duration for each measurement was usually between 5 and 6 min, while the subject stayed in the same position and his blood pressure was monitored simultaneously by the system as well as by the manual device, which provided measurement every minute.

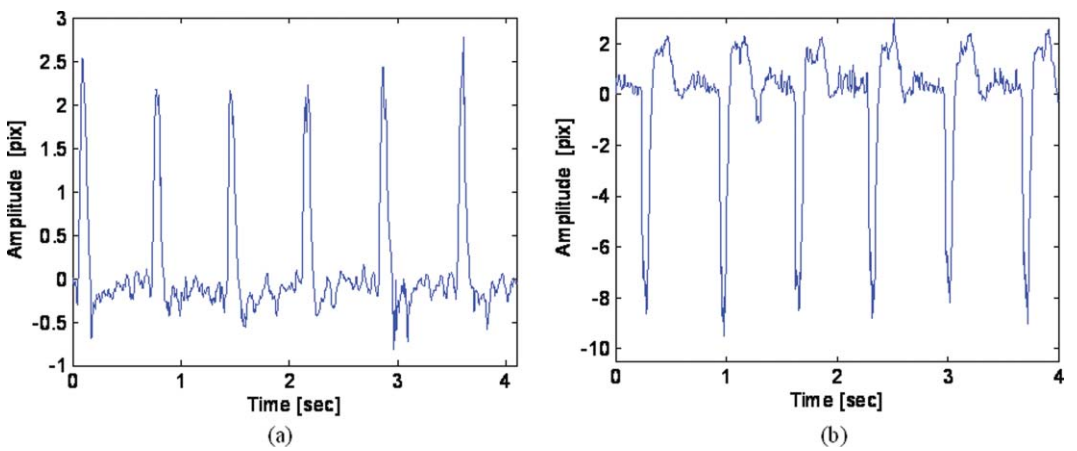

Fig. 2 Temporal plots of the outcome from the system used in the clinical trials for two different participants (a) and (b). In the charts, we present the amplitude of the relative shift of the speckle pattern between two subsequent frames.

The measurement duration was enough to monitor changes in blood pressure caused by exercising. Eventually, the measurement was ended when the blood pressure reached its original level. Longer time measurement will be possible in the future (aimed for patients with hypertension) by adjusting the proposed setup to the human wrist, therefore providing the subject the ability to move freely. This adjustment will also provide measurements with invariance to patient movements, as the relative angle between the device and the wrist will not change.

The following tests were performed to verify the reliability of the system: scalability, repeatability, stability and verification. The scalability test was aimed to determine whether the system product remains similar for different subjects. Ten subjects were tested under similar conditions. All subjects were healthy nonsmoker males, from 25 to 35 years old, with average fitness conditions. The repeatability test was aimed to determine whether the system results are stable in time. Two of the subjects participated in the experiment for a period of 1 yr to check it. They repeated the same test at least six times, while each test was performed every 2 months. The stability test was aimed to determine whether the system could produce constant results under constant blood pressure (before actual exercising of a subject). The verification test aimed to show a strong statistical basis for the correlation measurement and to distinguish the results from possible matching with other parameters.

4 Results

Figure 4 shows a typical outcome of the system. The figure is similar to Fig. 3, but this time both the *X* and *Y* axes of the correlation peak shift are shown, while the values are scaled to blood pressure units. One axis is better than the other with respect to the correlation with the pulse pressure (the difference between systolic and diastolic blood pressure is denoted by Δ) and its standard deviation error. Taking into account that the subject does not change orientation toward the laser illumination during a single test, the best correlation axis was chosen and used automatically in all the other measurements. The best correlation

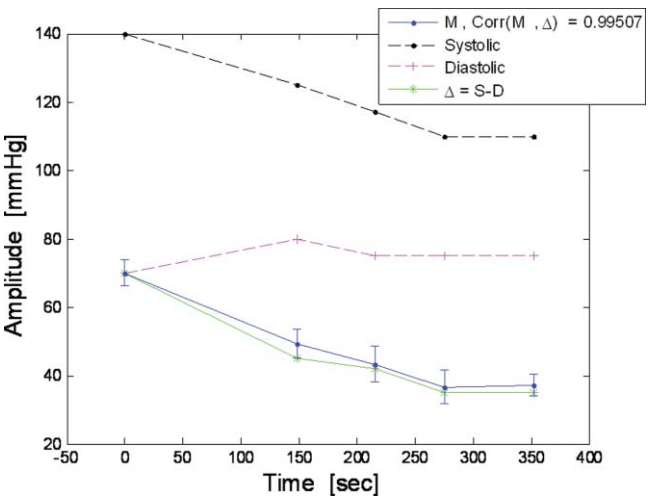

Fig. 3 Example of the obtained measurement for one subject participating in the clinical test group. The time duration is 350 s. The camera sampling was performed at 300 Hz.

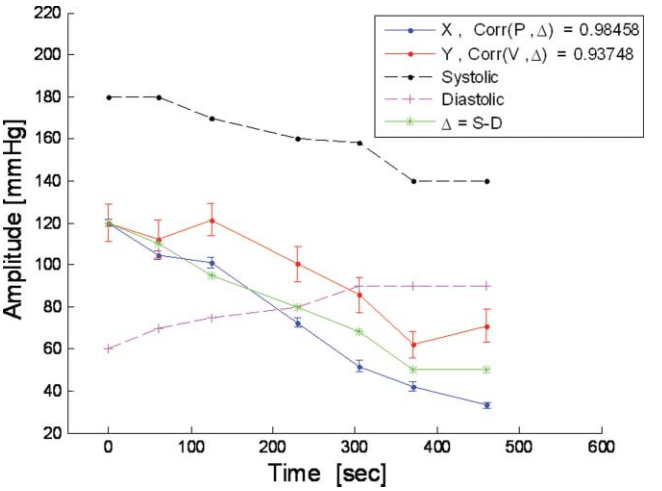

Fig. 4 Blood pulse pressure measurements performed over the clinical trial for the first subject. In the chart, we present the matching between the optical measurements obtained from both the *X* and *Y* axes and the reference measurement obtained using the conventional measurement technique.

axis was calibrated for each subject in each of the performed tests. The best axis remained stable during constant conditions. Thus, in Fig. 4, the *X* axis (appears under Δ-line) provides a better correlation factor of 0.985 with a smaller measurement error, while the *Y* axis (appears above Δ-line) provides correlation coefficient of only 0.937 with a larger measurement error (standard deviation). All the results that follow refer to the subjects' best axis, although this is not explicitly mentioned in the charts.

In the following we summarize the results of each of the performed tests.

4.1 *Scalability*

Figure 5 presents concentration of blood pressure measurements that were performed over the clinical trial group of

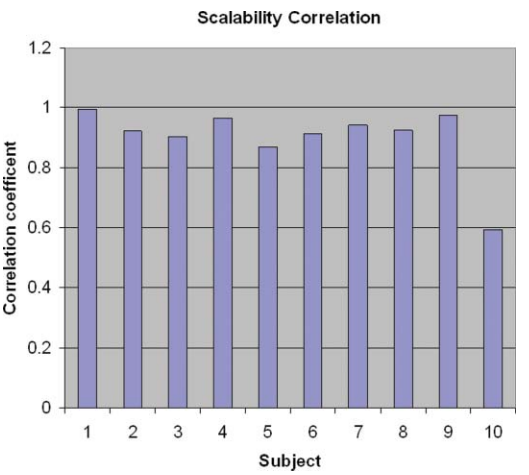

Fig. 5 Scalability test: a concentration of blood pulse pressure measurements performed over clinical trial group of 10 participants. The chart presents the matching (correlation coefficient) between the optical measurement and the reference measurement obtained using the conventional measurement technique.

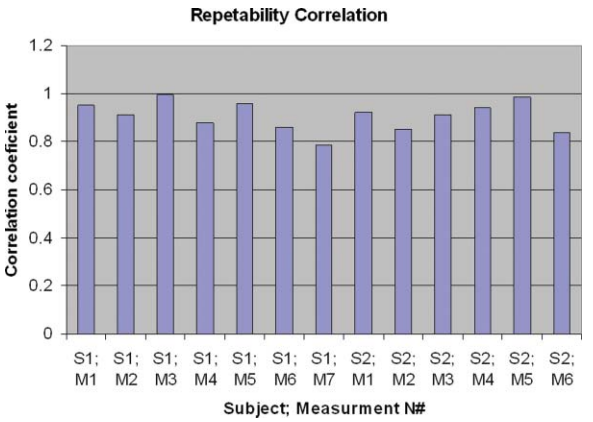

Fig. 6 Repeatability test: a concentration of blood pulse pressure measurements performed repeatedly for two participants in the clinical trials over a time period of 1 yr: S1, refers to subject number 1; M1, measurement number 1.

10 participants. In the chart, we present the match (correlation coefficient) between the optical measurement and the reference measurement obtained using the conventional blood pressure measurement technique, as already mentioned. One can see that 9 out of 10 subjects obtained correlation coefficients above 0.9. Only one subject had a correlation coefficient value of 0.6.

4.2 *Repeatability*

Repeatable blood pulse pressure measurements were performed with two participants over 1 yr. Figure 6 presents the results. Again, in the chart we present the matching (correlation coefficient) between the optical measurement and the reference measurement obtained using the conventional measurement technique. In the figure, S1 refers to subject number 1, M1 refers to measurement number 1, etc. One can see that 8 out of 13 measurements have correlation coefficients higher than 0.9,

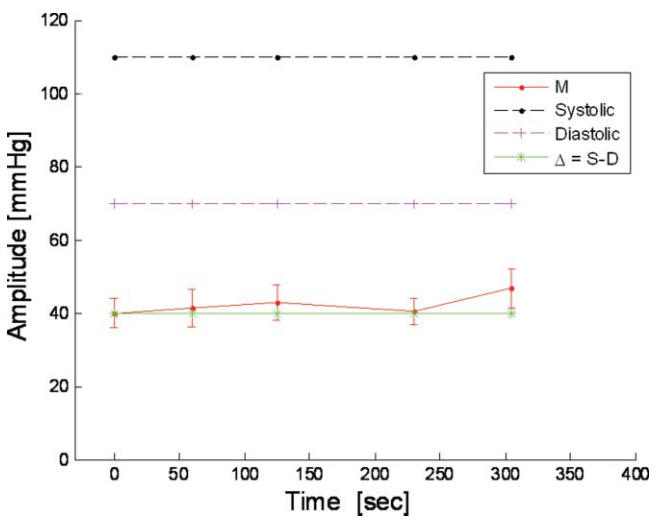

Fig. 7 Stability test: constant blood pulse pressure measurements (the subject was at rest) performed with the first subject participating in the clinical trials. In the chart, we present the match between optical measurement from the *X* axis and the reference measurement obtained using the conventional measurement technique.

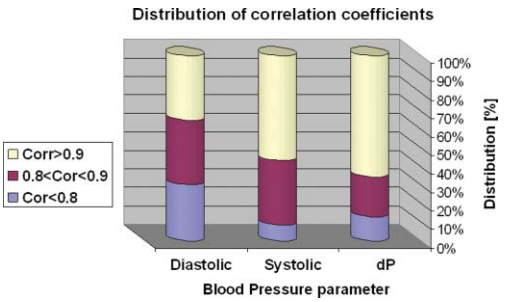

Fig. 8 Verification test: the distribution of the correlation coefficients obtained with clinical trial group of 10 participants. Three blood pressure parameters were tested.

and all measurements except one have correlation coefficients above 0.8.

4.3 *Stability*

The stability test included blood pulse pressure measurements, which were performed in our clinical trial for all subjects for constant blood pressure (when the subjects were at rest). Figure 7 presents the match between the optical measurement from the best axis and the reference measurement obtained using the conventional measurement technique for subject number 1. One can see that the *X* axis (this was chosen as the best axis and is denoted here by M) is relatively stable and it varies by no more than 15%. All subjects passed this test with variations below 15%.

4.4 *Verification*

A blood pulse pressure correlation distribution was computed for the clinical trial group of 10 participants and is presented in Fig. 8. In the chart, one can see a distribution of the correlation coefficients between the optical measurement and the reference measurement obtained using the conventional measurement technique. Three blood pressure parameters were checked: diastolic, systolic, and pulse pressure (d*P*). In blue (lower part), one can see a percentage of lower correlation coefficients that are below 0.8. In red (middle part), one can see a percentage of intermediate correlation coefficients that fall between 0.8 and 0.9. In yellow (higher part), one can see high correlation coefficient, which are above 0.9. Diastolic pressure was uniformly distributed and it does not present a good statistical property. Systolic pressure has more intermediate values and fewer high correlation coefficients. The pulse pressure (d*P*) presented the highest correlation coefficients for the implemented remote measurement technique.

5 Conclusions

We presented the usage of a recently developed optical configuration for remotely "hearing" heart beats for the estimation of blood pulse pressure. The system was tested with a clinical trial group, and the extracted results were compared with reference measurements obtained by conventional means.

We were able to demonstrate that by observing the amplitude of the correlation peak and not only its frequency or its position provides a measurement that is proportional to the difference

between the systolic and the diastolic blood pressure, i.e., the blood pulse pressure.

This new technique represents an inexpensive method for remote measurement of blood pulse pressure, providing a powerful diagnostic tool. In the performed testing, we used low emitted laser power, which is not more than several milliwatts. Further developments of currently presented technology will enable implementation of a multichannel and real-time monitoring device, which will be capable of analyzing pulse and blood pressure parameters in real time while allowing free movement of the subject.

References

1. H. Sorvoja and R. Myllylä, "Noninvasive blood pressure measurement methods," *Molec. Quantum Acoust*. **27**, 239–264 (2006).
2. J. G. Webster, *Medical Instrumentation Application and Design*, 4th ed., Wiley, New York (2009).
3. K. J. Fleckenstein, "The Mosso plethysmograph in 19th century physiology," *Med. Instrum.* **18**, 330–331 (1984).
4. J. Spigulis, "Optical noninvasive monitoring of skin blood pulsations," *Appl. Opt.* **44**, 1850–1857 (2005).
5. J. Spigulis, L. Gailite, A. Lihachev, and R. Erts, "Simultaneous recording of skin blood pulsations at different vascular depths by multiwavelength photoplethysmography," *Appl. Opt.* **46**, 1754–1759 (2007).
6. J. Allen, "Photoplethysmography and its application in clinical physiological measurement," *Physiol. Meas.* **28**, R1–R39 (2007).
7. H. Hong and M. Fox, "No touch pulse measurement by optical interferometry," *IEEE Trans. Biomed. Eng.* **41**, 1096–1099 (1994).
8. H. D. Hong and M. Fox, "Noninvasive detection of cardiovascular pulsations by optical Doppler techniques," *J. Biomed. Opt.* **2**, 382–390 (1997).
9. K. Meigas, H. Hinrikus, R. Kattai, and J. Lass, "Self-mixing in a diode laser as a method for cardiovascular diagnostics," *J. Biomed. Opt.* **8**, 152–160 (2003).
10. L. Scalise and U. Morbiduccia, "Non-contact cardiac monitoring from carotid artery using optical vibrocardiography," *Med. Eng. Phys.* **30**, 490–497 (2008).
11. C. Takano and Y. Ohta, "Heart rate measurement based on a time-lapse image," *Med. Eng. Phys.* **29**, 853–857 (2007).
12. T. Matsui, M. Uenoyama, H. Ishimine, S. Suzuki, K. Yamanaka, and M. Ishihara, "Non-contact determination of arterial blood pressure alterations induced by blood loss using laser irradiation on the common carotid artery," *J. Med. Eng. Technol.* **32**, 216–220 (2008).
13. R. Erts, U. Rubins, and J. Spigulis, "Monitoring of blood pulsation using non-contact technique," *IFMBE Proc.* **25**(VII), 754–756 (2009).
14. V. V. Tuchin, A. V. Ampilogov, A. G. Bogoroditsky, E. M. Rabinovich, V. P. Ryabukhov, S. S. Ul'yanov, and M. E. V'yushkin, "Laser speckle and optical fiber sensors for micromovements monitoring in biotissue," *Proc. SPIE* **1420**, 81–92 (1991).
15. S. S. Ul'yanov, V. P. Ryabukho, and V. V. Tuchin, "Speckle interferometry for biotissue vibration measurement," *Opt. Eng.* **33**, 908–914 (1994).
16. J. C. Dainty, *Laser Speckle and Related Phenomena*, 2nd ed., Springer-Verlag, Berlin (1989).
17. H. M. Pedersen, "Intensity correlation metrology: a comparative study," *Opt. Acta* **29**, 105-118 (1982).
18. P. K. Rastogi, and P. Jacquot, "Measurement on difference deformation using speckle interferometry," *Opt. Lett.* **12**, 596–598 (1987).
19. J. A. Leedertz, "Interferometric displacement measurements on scattering surfaces utilizing speckle effects," *J. Phys. E Sci. Instrum.* **3**, 214–218 (1970).
20. W. H. Peters and W. F. Ranson, "Digital imaging techniques in experimental stress analysis," *Opt. Eng.* **21**, 427–431 (1982).
21. N. Takai, T. Iwai, T. Ushizaka, and T. Asakura, "Zero crossing study on dynamic properties of speckles," *J. Opt. (Paris)* **11**, 93–101 (1980).
22. T. C. Chu, W. F. Ranson and M. A. Sutton, "Applications of digital-image-correlation techniques to experimental mechanics," *Exper. Mechan.* **25**, 232–244 (1985).
23. K. Uno, J. Uozumi, and T. Asakura, "Correlation properties of speckles produced by diffractal-illuminated diffusers," *Opt. Commun.* **124**, 16–22 (1996).
24. Z. Zalevsky and J. Garcia, "Motion detection system and method," Israeli Patent Application No. 184868 (July 2007); WO/2009/013738 International Application No. PCT/IL2008/001008 (July 2008).
25. Z. Zalevsky, Y. Beiderman, I. Margalit, S. Gingold, M. Teicher, V. Mico, and J. Garcia, "Simultaneous remote extraction of multiple speech sources and heart beats from secondary speckles pattern," *Opt. Express* **17**, 21566–21580 (2009).
26. W. R. Milnor, *Hemodynamics*, 2nd ed., Williams & Wilkins, Baltimore, MD (1982).
27. V. L. Streeter, *Fluid Mechanics*, Example 3.5, McGraw–Hill, New York (1966).